Redox Behavior and Kinetics of Hydroxo Ligand Exchange on Iron Tetraphenylporphyrin. Comparison with Chloro Exchange and Consequences for its Role in Self-Modulation of Molecular Catalysis of Electrochemical Reactions

Camille Chartier, Sylvie Chardon-Noblat, Cyrille Costentin

Redox Behavior and Kinetics of Hydroxo Ligand Exchange on Iron Tetraphenylporphyrin. Comparison with Chloro Exchange and Consequences for its Role in Self-Modulation of Molecular Catalysis of Electrochemical Reactions.

Camille Chartier, Sylvie Chardon-Noblat and Cyrille Costentin*

Univ Grenoble Alpes, DCM, CNRS, 38000 Grenoble, France.

Supporting Information

ABSTRACT: Thermodynamics and kinetics of hydroxide ion binding to iron tetraphenylporphyrin (TPPFe) at different redox states is investigated by electrochemistry and UV-vis spectroscopy. The reduction of TPPFe drastically decreases the binding affinity of hydroxide ions. An activation-driving force correlation is revealed showing that the strongest the binding affinity, the largest the association rate constant and vice-versa. Comparison with chloride ions shows that hydroxide ions are stronger ligands for iron tetraphenylporphyrin. However, kinetic data indicate that coordination and de-coordination of chloride ions is intrinsically faster than coordination and de-coordination of hydroxide ions. Finally, the consequence of hydroxide ion binding dynamics when TPPFe is used as a molecular catalyst for electrochemical reactions liberating hydroxides is discussed in the framework of self-modulation of catalytic processes.

Introduction

Transition metal coordination complexes are widely used as molecular catalysts for electrochemical transformations with particular interest for small molecule activation in the context of contemporary energy challenges. [1] They indeed present several interesting features such as the ability to cycle over many coordinated metal redox states and the possibility to fine tune their redox properties through ligand modifications. [2] Nonetheless, for a transition metal complex to be a chemical catalyst, i.e., activate a substrate via an innersphere process, it is required that a vacant coordination site is created and regenerated in the catalytic cycle. We have recently shown that ligand exchanges (Cl^-/OH^-), at the metal center of a bipyridyl tricarbonyl rhenium complex, play a crucial role in the modulation of the catalysis of nitrous oxide reduction.[3] A self-modulation process is indeed at play because the hydroxide ion, a co-product of the reaction, binds to the rhenium and prevents regeneration of the free coordination site unless more energy is injected in the system. Similar effects can also be found in other systems such as thus for the electrochemical reduction of CO_2 to CO catalyzed by $[Ni(cyclam)]^{2+}$ molecular catalyst partially inhibited by the formation of $[Ni(cyclam)(CO)]^+$ [4] or, thus for the reductive cleavage of chloroacetonitrile catalyzed by Co(I) cobalamins and cobinamides slowed down by free chlorides, produced by the reaction, binding to the catalyst.[5] When ligand exchange is involved in a catalytic cycle, the thermodynamics and kinetics of the corresponding steps may indeed play a role in the overall catalyst efficiency, either showing up in the turnover frequency or in the overpotential. It is thus important to quantitatively evaluate the thermodynamic and kinetic characteristics of ligand exchange processes at various redox states of a given complex and a given ligand.

Iron tetraphenylporphyrins (TPPFe) are well-studied molecular catalysts for small molecule activation, in particular dioxygen reduction to water at the level of the formal Fe(III)/Fe(II) redox couple [6] and carbon dioxide reduction to carbon monoxide at the level of the formal Fe(I)/Fe(0) redox couple. [7] Even at the level of the Fe(II)/Fe(I) redox couple, provided an appropriate modification of the ligand environment is designed. [8] Recently, TPPFe(0) has also been shown to trigger nitrous oxide reduction. [9] All these reactions involve a deoxygenation process, usually assisted by protons, and likely generating hydroxide ions, known as ligands for iron porphyrins. Hydroxide iron tetraphenylporphyrin TPPFe(OH) complexes may therefore be intermediates involved in the catalytic cycles of the above-mentioned reactions as well as in other reactions. Thereafter we report on the reduction of TPPFe(III)(OH) in dimethylformamide (DMF) with the aim to characterize thermodynamically and kinetically the ligand exchange processes at various redox states. While TPPFe(OH) has been studied for a long time, in particular in relation with the formation of μ-oxo dimer, [10] coordination and de-coordination properties of the hydroxo ligand have not been quantitively characterized. The influence of the latter properties on the electrochemical behavior of TPPFe, cycling between Fe(III) and Fe(0) formal states, will be described in the framework of the ladder eight members scheme shown in Scheme 1. We will then compare the properties of hydroxides vs. chlorides as axial ligands [11] and discuss the consequences coordination of hydroxide ions might have when TPPFe is used as a molecular catalyst for electrochemical reactions with particular emphasis on the self-modulation processes.

Results

Thermodynamics and UV-vis characterizations

In the absence of any axial coordinating ligand besides the solvent (DMF), TPPFe(III) exhibits three successive one electron reversible reduction waves in DMF + 0.1 M KPF_6 electrolyte as

attested by the cyclic voltammetry curve (CV) or linear scan voltammetry (LSV) on a rotating disk electrode (figure 1). DMF axial ligands are not explicitly considered throughout the paper. The standard potentials of corresponding formal TPPFe(III)/(II), TPPFe(II)/(I) and TPPFe(I)/(0) redox couples are at $E^0_{III/II}$ = -0.185, $E^0_{II/I}$ = -1.165 and $E^0_{I/0}$ = -1.840 V vs. SCE respectively (in agreement with literature data [12]), thus giving three of the ten thermodynamic constants of the ladder shown in Scheme 1.

Scheme 1.

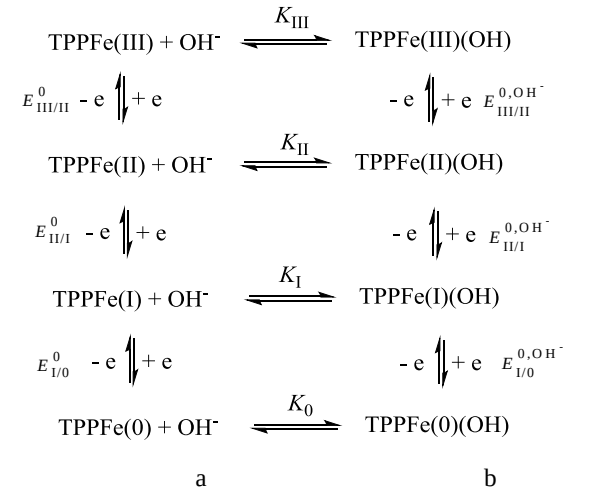

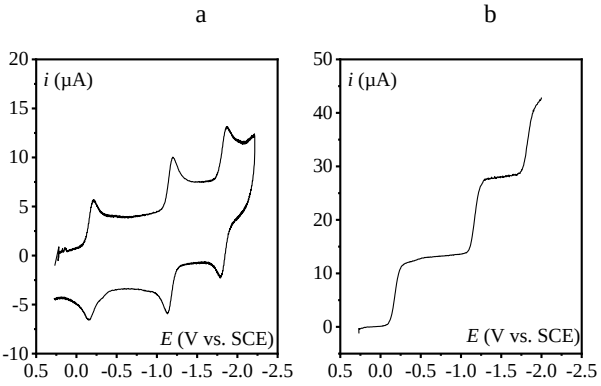

Figure 1. TPPFe(III) (0.5 mM) in DMF + 0.1 M KPF_6 under Ar on a 3 mm diameter GCE (a) CV at 0.1 V/s. (b) LSV at 2000 rpm and 0.01 V/s.

Starting from TPPFe(III), a one-electron exhaustive electrolysis is performed at -0.72 V vs. SCE leading quantitatively to a 0.5 mM solution of TPPFe(II). Then, successive additions of Et_4NOH (from 0.54 mM to 27 mM; i.e. ≈ 1 to 54 mole equivalents with respect to TPPFe) allows a progressive conversion of TPPFe(II) to TPPFe(II)(OH) followed by UV-vis (figure 2a). The characteristic Q-bands of both TPPFe(II) and TPPFe(II)(OH) are gathered in table S1. Their equilibrium concentrations can be calculated for each concentration of added hydroxides (figure 2b) and, considering the equilibrium corresponding to equation (1), the equilibrium constant K_{II} can be evaluated as K_{II} = 630 M^{-1} (see Supporting Information (SI) for details).

$$TPPFe(II) + OH^- \underset{k_b^{II}}{\overset{k_f^{II}}{\rightleftharpoons}} TPPFe(II)(OH) \qquad (1)$$

In the presence of an excess of OH^-, the reversible CV wave of Fe(III)/Fe(II) couple is shifted toward cathodic potentials (figure 3a) due to the stronger affinity of TPPFe(III) with hydroxide ions compared to TPPFe(II). The corresponding standard potential $E^{0,OH^-}_{III/II}$ is -0.815 V vs. SCE compared to $E^0_{III/II}$ = -0.185 V vs. SCE. Considering the thermodynamical relationships within a square diagram, we have:

$$E^{0,OH^-}_{III/II} = E^0_{III/II} + \frac{RT}{F}\ln\left(\frac{K_{II}}{K_{III}}\right) \qquad (2)$$

and therefore, we obtain K_{III} = 2.4 10^{13} M^{-1} >> 1 corresponding to the equilibrium constant of equation (3) and leading to the full thermodynamic characterization of the first square scheme of the ladder.

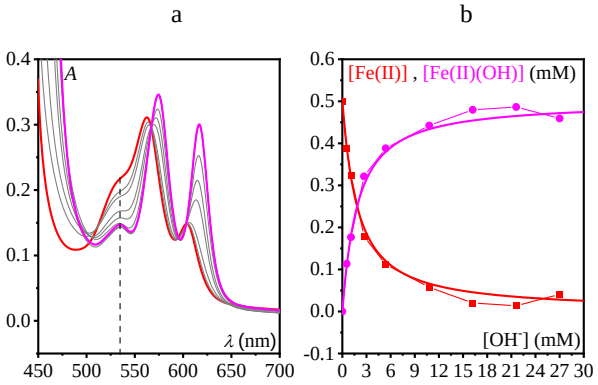

Figure 2. (a) in-situ evolution of UV-vis spectra (Q-bands *l*= 1 mm) of a solution of TPPFe(II) (0.5 mM) upon successive additions of Et_4NOH in DMF + 0.1 M KPF_6 under Ar; the initial TPPFe(II) spectrum is in red and the final spectrum is in magenta. ([Et_4NOH] = 27 mM). (b) Equilibrium concentrations of TPPFe(II) (red) and TPPFe(II)(OH) (magenta) as function of added Et_4NOH concentration.

In agreement with this very large binding constant, addition of OH^- on TPPFe(III) leads to quantitative transformation to TPPFe(III)(OH) as observed in UV-vis. (figure 3b). The UV-vis exhibits two Q-bands at 570 and 610 nm in agreement with literature data. TPPFe(III)OH is expected to evolve over time to form a µ-oxo dimer which UV-vis spectrum is expected to be similar to the UV-vis spectrum of TPPFe(OH) although with broader bands and a bathochromic shift. [13,14] However, we do not observe any change in UV-vis (and CV) over 3 hours (figure S1). Moreover, the EPR spectrum recorded at 100 K is similar to those reported for a monomeric high spin TPPFe(III)(OH) with effective g values 6.56, 5.75 and 1.98 (figure S2) whereas a µ-oxo dimer would not show EPR features. [13,14]

$$TPPFe(III) + OH^- \underset{k_b^{III}}{\overset{k_f^{III}}{\rightleftharpoons}} TPPFe(III)(OH) \qquad (3)$$

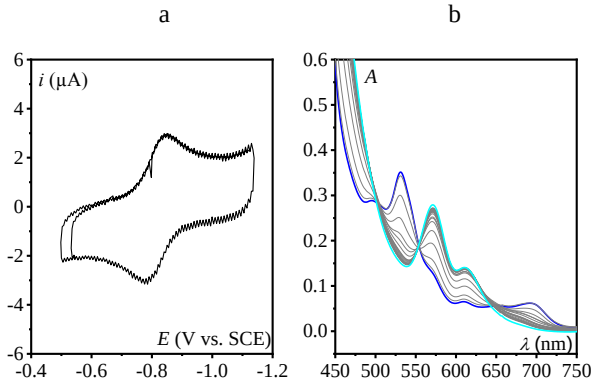

Figure 3. TPPFe(III) (0.5 mM) in DMF + 0.1 M KPF_6 under Ar (a) CVs at 0.1 V/s on a 3 mm diameter GCE in the presence of 27 mM of Et_4NOH. (b) Time evolution of UV-vis spectrum (Q-bands, *l*= 1 mm) upon addition of 0.54 mM Et_4NOH; the initial spectrum is in dark blue and the final spectrum is in light blue after 80 s.

Still in the presence of an excess of hydroxide ions, the reduction wave of TPPFe(II)(OH) occurs at more negative potential compared to the reduction of TPPFe(II) (-1.46 V vs. SCE ; figure 4a, peak 1). The wave is not reversible because of the kinetically limiting coordination of hydroxides to TPPFe(I) as discussed in more detail in the kinetic section. Nonetheless a partial reversibility is observed with a small kinetic anodic wave at ca. -1.40 V vs. SCE (peak 2 in figure 4a) hence leading to an estimation of the standard potential $E^{0,OH^-}_{II/I}$ in the range of -1.50 V vs. SCE. Thus, considering again a thermodynamical relationship within a square diagram, we have:

$$E^{0,OH^-}_{II/I} = E^{0}_{II/I} + \frac{RT}{F}\ln\left(\frac{K_I}{K_{II}}\right) \qquad (4)$$

leading to $K_I << 1\ M^{-1}$ for the equilibrium constant of equation (5). These values will be refined latter on when analyzing the kinetics of reaction (5).

$$TPPFe(I) + OH^- \underset{k_b^I}{\overset{k_f^I}{\rightleftarrows}} TPPFe(I)(OH) \qquad (5)$$

This gives a thermodynamic characterization of the second square scheme of the ladder.

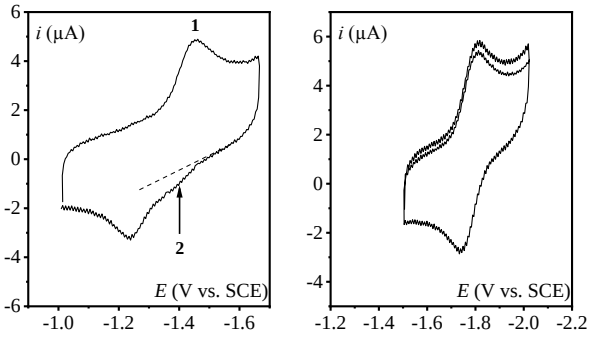

Figure 4. CVs recorded in DMF + 0.1 M KPF_6 under Ar at 0.1 V/s on a 3 mm diameter GCE in the presence of 27 mM of Et_4NOH containing (a) TPPFe(II)(OH) (0.5 mM). (b) TPPFe(I) (0.5 mM).

Regarding the lower square scheme of the ladder in Scheme 1, no information have been obtained concerning the hypothetical TPPFe(0)(OH) species. Even in the presence of excess of hydroxide ions (27 mM), de-coordination of OH^- occurs at the level of Fe(I) and the TPPFe(I)/TPPFe(0) wave remains unchanged (figure 4b). [15] No attempt was made to add larger excess of hydroxide ions. Based on the equilibrium constant estimated above, even at 1 M of hydroxides, less than 1 % of TPPFe(I) at 0.5 mM would be converted to TPPFe(I)(OH).

Kinetics

The thermodynamic binding constant of hydroxide ions to TPPFe(III) is so large ($K_{III} = 2.4\ 10^{13}\ M^{-1}$) that addition of hydroxide ions at 0.54 mM on a solution of 0.5 mM TPPFe(III) leads to a quantitative conversion to TPPFe(III)(OH) after less than 80 s as already shown in figure 3b. The time evolution of the absorbance at 702 nm, upon addition of hydroxide ions (0.54 mM) on a solution of 0.5 mM TPPFe(III) allows to extract the rate constant $k_f^{III} = 2000\ M^{-1}\ s^{-1}$ corresponding to the forward direction of reaction (3) considering initial conditions where [TPPFe(III)] ; [OH^-] and therefore (see figure 5 and SI for details):

$$\frac{[TPPFe(III)]_{t=0}}{[TPPFe(III)]} = 1 + k_f^{III}[TPPFe(III)]_{t=0}\,t \qquad (6)$$

Consequently, the backward rate constant of reaction (3), corresponding to the de-coordination of hydroxide ions from TPPFe(III)(OH) is as slow as $k_b^{III} = 7.15\ 10^{-11}\ s^{-1}$.

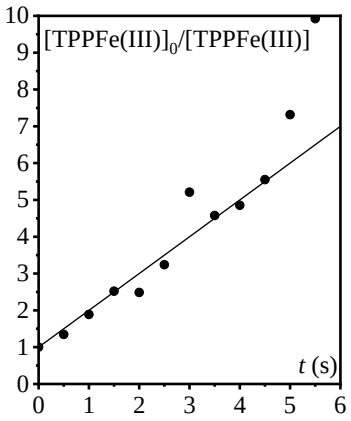

Figure 5. Time evolution of the inverse of the concentration of TPPFe(III) (initially 0.5 mM) in DMF + 0.1 M KPF_6 under Ar in the presence of 0.54 mM Et_4NOH. Linear fitting according to equation (6) (see SI for details).

The thermodynamic binding constant of hydroxide ions to TPPFe(II) is only K_{II} = 630 M^{-1} so that an excess of hydroxides is required to fully convert 0.5 mM of electrogenerated TPPFe(II) to TPPFe(II)(OH) (figure 2). As seen in figure 6, upon addition of 54 mM of Et_4NOH to 0.5 mM of TPPFe(II) generated by an exhaustive electrolysis of a TPPFe(III) solution at -0.82 V vs. SCE, complete conversion of TPPFe(II) to TPPFe(II)(OH) is obtained within less than 10 seconds.

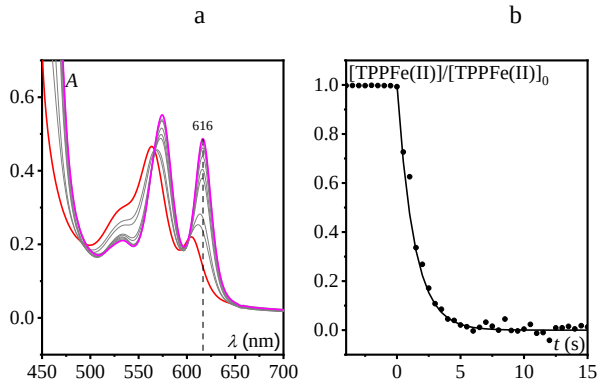

Figure 6. TPPFe(II) upon addition of 54 mM Et_4NOH in DMF + 0.1 M KPF_6 under Ar (a) Time evolution of UV-vis spectrum (Q-bands, *l*= 1 mm) ; the initial spectrum is in red and the final spectrum is in magenta. (b) Time evolution of the concentration of TPPFe(II). Fitting according to equation (7) (see SI for details).

From the time evolution of the absorbance at 616 nm, a pseudo-first order rate constant can be obtained leading to the rate constant k_f^{II} = 25 M^{-1} s^{-1} corresponding to the forward direction of reaction (2) (see figure 6b and SI for details):

$$\frac{[\mathrm{TPPFe(II)}]}{[\mathrm{TPPFe(II)}]_{t=0}} = \exp\left(-k_f^{II}\left[\mathrm{OH^-}\right]t\right) \qquad (7)$$

Hence, the backward rate constant of reaction (2), corresponding to the de-coordination of hydroxides from TPPFe(II)(OH) is k_b^{II} = 0.04 s^{-1}.

The thermodynamic binding constant of OH^- to TPPFe(I) is so small ($K_I << 1$ M^{-1}) that, as already indicated, preparation of TPPFe(I)(OH) from TPPFe(I) would require an excessively large amount of hydroxide ions. Therefore, to get insights into the dynamic of reaction (5), we consider the effect of the dynamics of this equilibrium on the cyclic voltammogram of TPPFe(II) reduction in the presence of Et_4NOH. As observed in figure 4a, only a small amount of TPPFe(II) is present according to K_{II} = 630 M^{-1} and noting that k_f^{II} = 25 M^{-1} s^{-1} and k_b^{II} = 0.04 s^{-1} lead to a quasi-frozen equilibrium on the timescale of a CV at 0.1 V/s. (i.e. $\frac{k_f^{II}\left[\mathrm{OH^-}\right]+k_b^{II}}{Fv/RT} < 1$).[16] The reduction wave is thus split in a first wave (peak 0 in figure 7) corresponding to the conversion of the fraction of TPPFe(II) to TPPFe(I) and a second wave (peak 1 in figure 4a and figure 7) corresponding to an EC mechanism leading predominantly to TPPFe(I) (scheme 2a). This second wave growth at the expand of the former as the amount of added hydroxide ions is increased. On the reverse scan the CV exhibits a weak wave at ca. -1.40 V vs. SCE corresponding to the oxidation of TPPFe(I) to TPPFe(II)(OH) via a CE process (scheme 2b, peak 2 in figure 4a and figure 7) whereas a second larger oxidation wave at a less negative potential corresponds to the EC pathway (scheme 2c, peak 3 in figure 7) leading to a mixture of TPPFe(II) and TPPFe(II)(OH) depending on the amount of hydroxides. Then a wave corresponding to TPPFe(III)(OH)/TPPFe(II)(OH) couple is observed (peaks 4 and 5 in figure 7). The position and shape of the waves corresponding to peaks 1 and 2 depends on the parameters $E_{II/I}^{0,OH^-}$, K_I and k_f^I (or k_b^I). Taking into account equation (4), only two parameters need to be adjusted to describe that position and shape of the waves. Using digital simulations (see SI), we roughly evaluate $E_{II/I}^{0,OH^-}$; -1.45 V vs. SCE, hence K_I ; 10^{-2} M^{-1}, and k_f^I ; 0.1 M^{-1} s^{-1} and k_b^I ; 10 s^{-1}. All equilibrium constants and rate constants are gathered in Table 1.

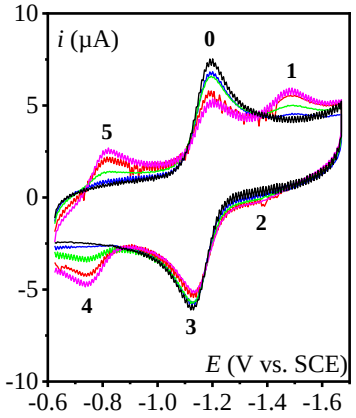

Figure 7. CVs recorded in DMF + 0.1 M KPF_6 under Ar at 0.1 V/s on a 3 mm diameter GCE in the presence TPPFe(II) (0.54 mM) and Et_4NOH: 0 (black), 0.54 (blue), 1.08 (green), 2.7 (red) and 5.4 mM (magenta); second cycles are shown.

Scheme 2.

a) reduction (EC), peak 1

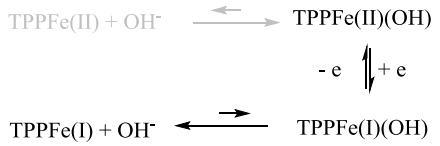

b) oxidation (CE), peak 2

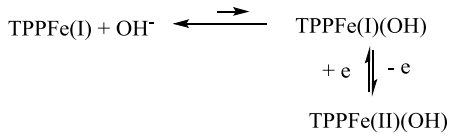

c) oxidation (EC), peak 3

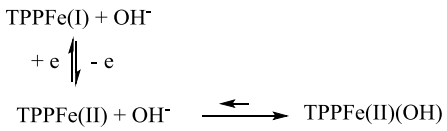

Discussion

A thermodynamic characterization of the ladder (Scheme 1) corresponding to TPPFe/TPPFe(OH) equilibrium at various redox states was performed. We took advantage of the fact that the equilibrium constant for hydroxide coordination/de-coordination is neither to large nor to small at the Fe(II) redox state to measure it by simple spectrometric titration. It would not have been possible at the TPPFe(III) redox state because the equilibrium constant for OH^- binding is too large and it would not have been possible at the TPPFe(I) redox state because the equilibrium constant for hydroxide binding is too small. However, as methodologically explained in reference 11, the determination of the differences of the standard potentials allows to derive these equilibrium constants via equations (2) and (4).

Table 1. Equilibrium and rate constants

ligand	OH^-	Cl^- [a]
Equilibrium constants		
K_{III} (M^{-1})	2.4 10^{13}	2.5 10^{5}
K_{II} (M^{-1})	630	56
K_{I} (M^{-1})	1.5 10^{-3}	-
Rate constants		
k_f^{III} ($M^{-1}s^{-1}$); k_b^{III} (s^{-1})	2000; 7.15 10^{-11}	9.6 10^{7}; > 4 10^{2}
k_f^{II} ($M^{-1}s^{-1}$); k_b^{II} (s^{-1})	25; 0.04	10^{5}; 2 10^{3}
k_f^{I} ($M^{-1}s^{-1}$); k_b^{I} (s^{-1})	0.1; 70	-

[a] from reference 11.

The very large value of K_{III} is in line with previously evaluated binding constants of the hydroxide ions with other iron(III)tetraphenylporphyrins protected from μ-oxo dimer formation with "basket-handle" type aliphatic hydrocarbon chains. Binding constant of the order of 10^{23} and 10^{20} M^{-1} have been reported in benzonitrile.[14] The binding affinity of OH^- dramatically decreases, by more than ten orders of magnitude; when TPPFe is reduced from Fe(III) to Fe(II) formal redox states. We also note that the equilibrium constant K_{II} is smaller than the corresponding constants evaluated with the protected "basket-handle" iron(II)tetraphenylporphyrins (1.6 10^3 and 2.3 10^6 M^{-1} vs 630 M^{-1} for K_{II}).[14] One explanation could be that, in the protected porphyrins, the aliphatic hydrocarbon chains are linked to the ortho positions of the phenyl groups by amides functionalities providing dipolar and H-bonding interactions stabilizing the hydroxo ligand. Reducing once more TPPFe to the Fe(I) formal state, again induced an important decrease of the binding affinity by several orders of magnitude. Interestingly, equilibrium constants have been previously determined for the binding of chloride ions to TPPFe(III) and TPPFe(II) (see Table 1).[11] In both cases, the binding affinity of Cl^- is smaller than the binding affinity of OH^- indicating that hydroxide is a stronger ligand for iron tetraphenylporphyrin than chloride.

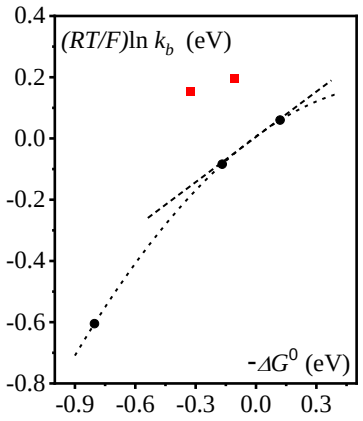

Figure 8. Activation ($\frac{RT}{F}\ln k_b^i$) - driving force ($-\Delta G^0 = RT \ln K_i$ with I = I, II or III) plot for ligand de-coordination from TPPFe(L) (L=OH^- in black, L=Cl^- in red). See Table 1 for data. Dashed line and curve: respectively linear and quadratic fitting of the activation-driving force correlation.

We have also been able to determine the rate constants for hydroxide coordination to and de-coordination from TPPFe at three different redox states. As expected, the strongest the binding affinity, the largest the association rate constant and vice-versa (Table 1). Therefore, an activation ($\frac{RT}{F}\ln k_b$) -driving force ($-\Delta G^0$) correlation can be drawn for the de-coordination processes. As shown in figure 8, around $\Delta G^0 = 0$, the transfer

coefficient $\alpha = \partial \Delta G^{\neq} / \partial \Delta G^{0}$ is equal to 0.5 whereas it is larger at unfavorable driving force. It is reminiscent of electron transfer [17] and dissociative electron transfer [18] activation-driving force relationships although the processes investigated here is a simple coordination chemistry reaction. De-coordination of chloride appears intrinsically faster than de-coordination of hydroxide because, for a similar driving force, the de-coordination rate is much faster (see figure 8). More investigation is required to get deeper insights in the intrinsic reasons for such a behavior but these results encourage us to seek more in that direction in future work. Dynamics of ligand coordination/de-coordination is indeed deemed to play an important role in catalytic processes involving coordination complexes as catalysts. Hence, we will now discuss the possible influence of the formation of TPPFe(II)(OH) on a catalytic process when TPPFe plays the role of molecular catalyst at the level of TPPFe(II)/TPPFe(I) couple for an electrochemical reaction involving a two electron reductive deoxygenation reaction with water as proton source (equation 8):

$$\text{Substrate} + 2\,e \xrightarrow[H_2O]{} \text{Product} + 2\,OH^- \qquad (8)$$

Typical examples would be the reduction of CO_2 to CO, recently shown to possibly occurs at the Fe(II)/Fe(I) redox couple of well-designed iron porphyrins [8]**Erreur ! Signet non défini.** or the reduction of N_2O to N_2; many other reactions corresponding to equation (8) can also be envisioned. We consider a simple mechanism depicted in Scheme 3 in which the rate determining step is the first chemical reaction involving the electrogenerated TPPFe(I) and the substrate to be reduced. Therefore, a steady-state approximation can be considered for the intermediate. If the reaction is performed in a range of potentials, in which TPPFe(II)(OH) cannot be directly reduced at the electrode (i.e. E > -1.4 V vs. SCE), the framework considered here corresponds to a self-modulation situation. Indeed, the catalytic reaction generates hydroxide ions which will slow down and eventually inhibits the reaction via the formation of TPPFe(II)(OH).

Scheme 3.

$$\text{TPPFe(II)} + e \rightleftharpoons \text{TPPFe(I)}$$

$$\text{TPPFe(I)} + \text{Substrate} \xrightarrow{k_1} \text{Intermediate}$$

$$\text{TPPFe(I)} + \text{Intermediate} \xrightarrow[H_2O]{k_2 >> k_1} 2\,\text{TPPFe(I)} + \text{Product} + 2\,OH^-$$

$$\text{TPPFe(II)} + OH^- \underset{k_b^{II}}{\overset{k_f^{II}}{\rightleftharpoons}} \text{TPPFe(II)(OH)}$$

To rationalize this effect, a kinetic analysis of such a self-modulation catalytic process can be performed within simplifying assumptions, such as excess of substrate and fast catalysis considering either cyclic voltammetry as an analytic technique, or constant potential electrolysis (CPE), with a controlled hydrodynamic regime (stirring of the solution). Fast catalysis corresponds in CV to the condition $\lambda_{CV} = \dfrac{k_{cat}}{Fv/RT} > 1$ with $k_{cat} = k_1 C^0_{substrate}$ and v the scan rate.[16] In CPE, fast catalysis corresponds to the condition $\lambda_{CPE} = \dfrac{k_{cat}}{D/\delta^2} > 1$ where D and δ are respectively the diffusion coefficient of TPPFe and the size of the diffusion layer in CPE, set by the stirring rate of the solution.[19] Because the rate constants for hydroxide coordination to and de-coordination from TPPFe(II) are relatively slow (k_f^{II} = 25 M^{-1} s^{-1} and k_b^{II} = 0.04 s^{-1}), we restrict our analysis to a situation where catalysis is fast (see above assumptions) and occurs in a thin diffusion-layer close to the electrode surface generating hydroxide ions that interfere with TPPFe(II) in the diffusion layer as well as in the bulk of the solution (in the case of CPE). In that context, as shown in the SI, considering first CV, the system is controlled by two dimensionless parameters $\sigma_{CV} = \dfrac{k_f^{II} C^0_{cat} \sqrt{2k_{cat}}}{(Fv/RT)^{3/2}}$ and $\rho_{CV} = K_{II} C^0_{cat} \sqrt{\dfrac{2k_{cat}}{Fv/RT}}$. If ρ_{CV} is large, a likely situation for fast catalysis taking into account that K_{II}=630 M^{-1} and that C^0_{cat} is typically in the sub-millimolar range, the coordination of OH^- to TPPFe(II) can be considered as irreversible on the timescale of the CV, hence making the CV dependent on a single parameter σ_{CV}. Simulations (see SI for details) of the corresponding dimensionless CVs, i.e., $\varphi = \dfrac{i}{FSC^0_{cat}\sqrt{D}\sqrt{2k_{cat}}}$ vs. $\xi = -\dfrac{F}{RT}\left(E - E^0_{II/I}\right)$) as function of the parameter σ_{CV} are shown in figure 9a. It is seen that an irreversible coordination of hydroxide ions to TPPFe(II) inhibits catalysis with a progressive departure of the current from the canonical S-shaped CV obtained in the absence of binding (σ_{CV} = 0). Note that the canonical CV can be reached at high scan rate, minimizing the inhibition process by decreasing the time scale of the CV and hence the charge passed and consequently the amount of OH^- produced.

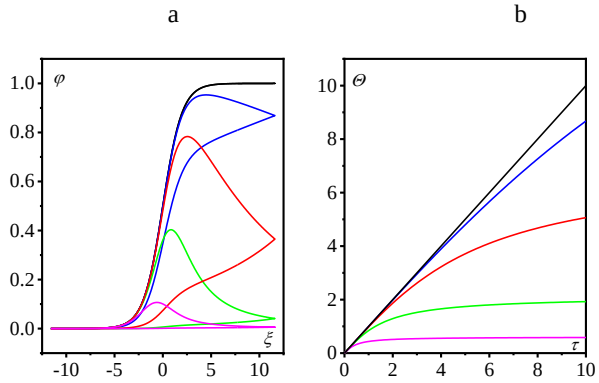

Figure 9. Effect of self-modulation on catalysis. (a) Dimensionless CVs corresponding to the mechanism in Scheme 3. $\varphi = \dfrac{i}{FSC^0_{cat}\sqrt{D}\sqrt{2k_{cat}}}$ vs. $\xi = -\dfrac{F}{RT}\left(E - E^0_{II/I}\right)$ for σ_{CV} = 0 (black), 0.01 (blue), 0.1 (red), 1 (green), 10 (magenta). (b) Dimensionless charge (Θ) vs. time (τ) passed in CPE at an applied potential $\xi_{applied} = -\dfrac{F}{RT}\left(E_{applied} - E^0_{II/I}\right) = 20$ and corresponding to the mechanism in scheme 3 for σ_{CPE} = 0 (black), 0.01 (blue), 0.1 (red), 1 (green), 10 (magenta).

Considering now a CPE, the effect of self-modulation of the catalysis due to an irreversible binding of hydroxide ions produced by the catalytic reaction to TPPFe(II) can be formally

monitored by looking at the dimensionless charge passed during electrolysis, $\Theta = \int_0^\tau \varphi d\tau$ vs. τ where the dimensionless time is $\tau = \frac{t}{V\delta / DS}$ (V is the volume of the electrolysis cell and S the surface area of the cathode). This dimensionless charge, $\Theta = \frac{Q}{FVC_{cat}^0 \delta / \sqrt{D / 2k_{cat}}}$ ($Q = \int_0^t idt$ is the actual charge passed), depends on a dimensionless parameter $\sigma_{CPE} = \frac{\delta^2 V}{D^{3/2} S} k_f^{II} C_{cat}^0 \sqrt{2k_{cat}}$ according to an analytical expression (see SI):

$$\Theta = \sqrt{\frac{2}{\sigma_{CPE}\left[1+\exp(-\xi)\right]}} \arctan\left(\tau \sqrt{\frac{\sigma_{CPE}}{2\left[1+\exp(-\xi)\right]}}\right) \quad (9)$$

and leading to:

$$\Theta_{max} = \Theta_{\tau\to\infty} = \frac{\pi}{\sqrt{2\sigma_{CPE}\left[1+\exp(-\xi)\right]}} \quad (10)$$

When $\sigma_{CPE} \to 0$, the charge passed increases linearly with time due to a sustained catalysis. Increasing values of σ_{CPE} leads to an increasing deviation from this behavior due to a decrease of the catalytic current induced by the inhibition of the catalyst via irreversible binding of hydroxide ions (figure 9b). A maximal charge can be passed (Θ_{max}) from which a maximal turnover number, $TON_{lim} = \frac{Q_{max}}{2FVC_{cat}^0} = \frac{\delta\Theta_{max}}{\sqrt{2D / k_{cat}}}$, can be evaluated. It corresponds to the maximal number of molecules of product formed (taking into account the stoichiometry of equation (8)) divided by the total amount of catalyst (TPPFe(II)) initially present in solution and eventually converted to TPPFe(II)(OH). When the applied potential is negative enough, then:

$$TON_{lim} = \frac{\pi}{2^{3/2}} \sqrt{\frac{S}{V} \frac{\sqrt{D}\sqrt{k_{cat}}}{k_f^{II} C_{cat}^0}} \quad (11)$$

As revealed by equation (11), TON_{lim} is not an intrinsic parameter of the chemical system, as opposed to the corresponding maximal turnover number reached when catalysis is limited by the degradation of the active form of the catalyst. In such a case, it has been shown that $TON_{lim} = \frac{k_{cat}}{k_i}$ where k_i is the first order apparent constant of degradation of the active form of the catalyst; [20] here we have evolution of the resting state of the catalyst. In self-modulation processes, besides intrinsic factors (k_{cat}, k_f^{II} and the diffusion coefficient D), TON_{lim} depends on operational factors, namely, the catalyst concentration and the characteristic cell length V / S. Importantly, the kinetics of ligand binding, via k_f^{II}, is crucial in modulating the catalysis efficiency. It is therefore important to gather kinetic information on ligand exchange reactions on catalysts as shown here in the case of hydroxide ions and TPPFe.

Conclusion

We have investigated the redox behavior of TPPFe in the presence of hydroxide ions. By a combination of electrochemical and UV-vis measurements, the binding affinity of hydroxides with TPPFe(III), TPPFe(II) and TPPFe(I) was measured as well as the corresponding coordination rate constants. As expected, the strongest the binding affinity, the largest the association rate constant. Comparison with existing values in the literature for chloro ligands reveals that de-coordination of chloride ions is intrinsically faster than de-coordination of OH^-.

TPPFe being widely used as a molecular catalyst for electrochemical reduction of substrates and in particular deoxygenation reactions generating hydroxides as co-product, we have investigated the possible influence of hydroxide coordination on TPPFe(II) when TPPFe(II)/TPPFe(I) would be the catalyst redox couple. Our analysis shows that a self-modulation process leads to inhibition of catalysis and that the maximal turnover number that can be reached in controlled potential electrolysis is strongly dependent on the rate constant of hydroxide ion binding to metallic center in TPPFe(II).

This study not only provides missing information on the redox behavior and kinetics of hydroxide coordination to TPPFe, but it also points out the crucial role of ligand exchange dynamics in the modulation of homogeneous molecular catalysis of electrochemical reactions.

ASSOCIATED CONTENT

Supporting Information

Experimental details. Details on determination of thermodynamic parameters and kinetic analysis. Formal kinetics.

ACKNOWLEGMENT

This work was supported by the Agence Nationale de la Recherche (DeNOSOr project ANR-22-CE07-0034-02), and Labex ARCANE (CBH-EUR-GS, ANR-17-EURE-0003). Ecole Normale Supérieure de Lyon is acknowledged for financial support for Camille Chartier. The NanoBio ICMG (UAR 2607) is acknowledged for providing facilities for NMR analyses. Florian Molton is warmly thanked for recording EPR spectra.

AUTHOR INFORMATION

Corresponding Author

cyrille.costentin@univ-grenoble-alpes.fr

Notes

The author declares no competing financial interest.

REFERENCES

1. (a) Savéant, J-M. Molecular Catalysis of Electrochemical Reactions. Mechanistic Aspects. *Chem. Rev.* **2008**, *108*, 2348-2378. (b) Dalle, K. E.; Warnan, J.; Leung, J. J; Reuillard, B.; Karmel, I. S.; Reisner, E. Electro- and Solar-Driven Fuel Synthesis with First Row Transition Metal Complexes. *Chem. Rev.* **2019**, *119*, 2752-2875.
2. See for example: (a) Clark, M. L.; Cheung, P. L.; Lessio, M.; Carter, E. A.; Kubiak, C. P. Kinetic and Mechanistic Effects of Bipyridine (bpy) Substituent, Labile Ligand, and Bronsted Acid on Electrocatalytic CO_2 Reduction by Re(bpy) Complexes. *ACS Catal.* **2018**, *8*, 2021-2029. (b) Azcarate, I.; Costentin, C. ; Robert, M. ; Savéant, J-M. Through-Space Charge Interaction Substituent Effects in Molecular Catalysis Leading to the Design of the Most Efficient Catalyst of CO_2-to-CO Electrochemical Conversion. *J. Am. Chem. Soc.* **2016**, *138*, 16639-16644.
3. Deeba, R.; Chardon-Noblat, S.; Costentin, C. Importance of Ligand Exchange in the Modulation of Molecular Catalysis: Mechanism of the Electrochemical Reduction of Nitrous Oxide with Rhenium Bipyridyl Carbonyl Complexes. *ACS Catal.* **2023**, *13*, 8262-8272.
4. Froehlich, J. D.; Kubiak, C. P. The Homogeneous Reduction of CO_2 by $[Ni(cyclam)]^+$: Increased Catalytic Rates with the Additionvof a CO Scavenger. *J. Am. Chem. Soc.* **2015**, *137*, 3565−3573.
5. Argüello, J. E.; Costentin, C.; Griveau, S.; Savéant, J-M. Role of Protonation and of Axial Ligands in the Reductive Dechlorination of Alkyl Chlorides by Vitamin B12 Complexes. Reductive Cleavage of Chloroacetonitrile by Co(I) Cobalamins and Cobinamides. *J. Am. Chem. Soc.* **2005**, *127*, 5049−5055.
6. (a) Oliveira, R.; Zouari, W.; Herrero, C.; Banse, F.; Schöllhorn, B.; Fave, C.; Anxolabéhère-Mallart, E. Characterization and Subsequent Reactivity of an Fe-Peroxo Porphyrin Generated by Electrochemical Reductive Activation of O_2. *Inorg. Chem.* **2016**, *55*, 12204-12210. (b) Bhunia, S.; Ghatak, A.; Rana, A.; Dey, A. Amine Groups in the Second Sphere of Iron Porphyrins Allow for Higher and Selective $4e^-/4H^+$ Oxygen Reduction Rates at Lower Overpotentials. Journal of the American Chemical Society **2023**, *145*, 3812-3825. (c) Pegis, M. L.; Martin, D. J.; Wise, C. F.; Brezny, A. C.; Johnson, S. I.; Johnson, L. E.; Kumar, N.; Raugei, S.; Mayer, J. M. Mechanism of Catalytic O_2 Reduction by Iron Tetraphenylporphyrin. *J. Am. Chem. Soc.* **2019**, *141*, 8315-8326.
7. Costentin, C.; Robert, M.; Savéant, J-M. Current Issues in Molecular Catalysis Illustrated by Iron Porphyrins as Catalysts of the CO_2-to-CO Electrochemical Conversion. *Acc. Chem. Res.* **2015**, *48*, 2996-3006.
8. Amanullah, S.; Gotico, P.; Sircoglou, M.; Leibl, W.; Llansola-Portoles, M. J.; Tibiletti, T.; Quaranta, A.; Halime, Z.; Aukauloo, A. Second Coordination Sphere Effect Shifts CO_2 to CO Reduction by Iron Porphyrin from Fe0 to FeI. *Angew. Chem. Int. Ed.* **2023**, e202314439.
9. Stanley, J. S.; Wang, X. S.; Yang, J. Y. Selective Electrocatalytic Reduction of Nitrous Oxide to Dinitrogen with an Iron Porphyrin Complex. *ACS Catal*., **2023**, *19*, 12617–12622.
10. Kadish, K. M.; Larson, G.; Lexa, D.; Momenteau, M. Electrochemical and Spectral Characterization of the Reduction Steps of µ-Oxo-bis(iron tetraphenylporphyrin) Dimer in Dimethylformamide. *J. Am. Chem. Soc.* **1975**, *97*, 282-.
11. Lexa, D.; Rentien, P.; Savéant, J-M.; Xu, F. Methods for investigating the mechanistic and kinetic role of ligand exchange reactions in coordination electrochemistry. Cyclic voltammetry of chloroiron(III)tetraphenylporphyrin in dimethylformamide. *J. Electronanal. Chem.* **1985**, *191*, 253-279.
12. Mitchell, N. H.; Elgrishi, N. Investigation of Iron(III) Tetraphenylporphyrin as a Redox Flow Battery Anolyte: Unexpected Side Reactivity with the Electrolyte. *J. Phys. Chem. C*, **2023**, *127*, 10938-10946.
13. Fielding, L.; Eaton, G. R.; Eaton, S. S. Mechanism of Conversion of Iron(III)Tetratolylporphyrin Hydroxide to the Corresponding µ-Oxo-Bridged Dimer. *Inorg. Chem.* **1985**, *24*, 2309-2312.
14. Lexa, D.; Momenteau, M.; Savéant, J-M.; Fu, F. Redox Properties and Stability of Hydroxy Complexes of Protected Iron(III) and Iron(II) Porphyrins. *Inorg. Chem.* **1985**, *24*, 122-127
15. A small anodic shift is observed indicating a stabilization of TPPFe(0) vs. TPPFe(I) in the presence of 27 mM Et_4NOH. It might be due to the presence of water that leads to a better solvation of the doubly negatively charged TPPFe(0) vs. the mono negatively charged TPPFe(I) in the presence of water.
16. Savéant, J-M.; Costentin, C. *Elements of Molecular and Biomolecular Electrochemistry*. 2nd Ed. Wiley, 2019. Chap. 2.
17. Marcus, R. A. On the Theory of Electron-Transfer Reactions. VI. Unified Treatment for Homogeneous and Electrode Reactions. *J. Chem. Phys.* **1965**, *43*, 679-701.
18. Savéant, J-M. A Simple Model for the Kinetics of Dissociative Electron Transfer in Polar Solvents. Application to the Homogeneous and Heterogeneous Reduction of Alkyl Halides. *J. Am. Chem. Soc.* **1987**, *109*, 6788-6795.
19. Deeba, R.; Collard, A.; Rollin, C.; Molton, F.; Chardon-Noblat, S.; Costentin, C. Controlled Potential Electrolysis: Transition from Fast to Slow Regimes in Homogeneous Molecular Catalysis. Application to the Electroreduction of CO_2 Catalyzed by Iron Porphyrin. *ChemElectroChem.* **2023**, e202300350.
20. Costentin, C.; Passard, G; Savéant, J-M. Benchmarking of Homogeneous Electrocatalysts: Overpotential, Turnover Frequency, Limiting Turnover Number. *J. Am. Chem. Soc.* **2015**, *137*, 5461-5467.

TOC

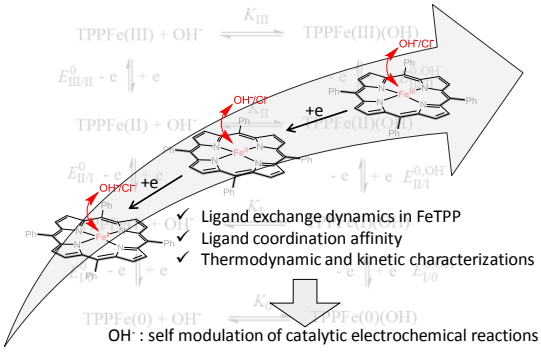

Synopsis: Thermodynamics and kinetics of hydroxide ion coordination to iron center of tetraphenylporphyrin (TPPFe) at different redox states is determined and shown to follow an activation-driving force correlation. Comparison with chloride coordination shows that the hydroxide is a stronger ligand for iron tetraphenylporphyrin although intrinsically less labile. Binding dynamics of hydroxide ions, produced by a catalytic reaction, is predicted to induce a self-modulation of molecular catalytic electrochemical processes kinetically modelled.